Journal of Materials Chemistry C

ARTICLE

Tunable optical properties of OH-functionalised graphene quantum dots

Received 00th June 2016,
Accepted 00th June 2016

DOI: 10.1039/x0xx00000x

www.rsc.org/

K. R. Geethalakshmi,[*a] Teng Yong Ng,[a] and Rachel Crespo-Otero[*b]

Graphene oxide quantum dots (**GO-QDs**) have distinct optoelectronic properties for their applications in bio-imaging, drug delivery and photovoltaics. Herein, the effect of OH functionalisation on optical properties of **GO-QDs** is studied based on state-of-the-art theoretical simulations. Our calculations predict a trend in the distribution of OH groups on ionisation potentials, light absorption and emission properties. The mechanism of fluorescence is analysed considering the role of geometry distortion and charge transfer. Moreover, selective functionalisation on positions with large electron-hole separation offers a strategy to tune the optical gap and photoluminescence properties. These results open up new opportunities for the design of **GO-QDs** for a wide range of applications.

A. Introduction

Graphene oxide (**GO**) is evolving as a multifaceted candidate material for optoelectronics,[1] next-generation ultrathin electronics,[2,3] energy conversion and storage technologies.[4–6] However, the underlying issue currently limiting the **GO**'s direct attachment to devices is the poor understanding to enforce spatial control over oxygen groups in the experimental processes.[7–9] These restrictions result in large optical gaps and drive poor electronic conductivity.[1,10,11]

GO has a strong absorption in the ultraviolet region showing energy shifts towards the visible with increasing level of oxidation.[12,13] **GO** contains oxygen mainly in the form of epoxy, hydroxyl and carboxyl functional groups on the basal plane and at the sheet edges. [7,14] Hydroxyl groups stabilise the surface, help radiative recombination and consequently enhance the fluorescence yield.[15–17] Selective chemical reduction of carboxyl and epoxy groups with $NaBH_4$ increases the fraction of hydroxyl groups.[17]

The photoluminescence properties of **GO** can be tuned from deep ultraviolet to near infrared by reducing the size to the nanoscale regime and by controlling edge configuration effects, functional groups and defects.[18] These so-called graphene oxide quantum dots (**GO-QDs**) have received considerable attention because of their distinct structural and optoelectronic properties and for their potential applications such as bio-imaging, drug delivery and photovoltaics.[19,20]

Synthesis methods have not been very successful in producing **GO-QDs** with controllable size or functionalities and reaction conditions strongly affect the absorption and emission spectra.[19,21] **GO-QDs**, in the range size of 1-4 nm, were synthesised by Peng *et al*. showing photoluminescence tunability.[22] The first absorption peak shifted from 330 to 270 nm when the temperature changed from 80 to 120 ˚C. Jang *et al*. synthesised **GO-QDs** with different amounts of oxygen using direct oxidation of graphite nanoparticles and by conventional chemical reduction.[19] **GO-QDs** of similar sizes obtained by different methods showed different carrier dynamics, but similar tendencies with regard to the oxygen composition.

In this context, the combined effects of oxygen content and size on the mechanisms of light absorption and luminescence are not well understood and inconsistent experimental outcomes undergo contradictory hypotheses due to large heterogeneity in synthesised **GO-QDs**. There are two interpretations of the mechanism of fluorescence: localization of sp^2 clusters and involvement of oxygen functional groups. Herein, we analyse both mechanisms based on state-of-the-art theoretical simulations.[21]

Theoretical calculations are particularly useful to isolate the effect of different factors contributing to a particular mechanism. Several groups have explored the properties of graphene quantum dots (**G-QDs**) using different levels of theoretical approximations.[18,23–31] Recently, Yamijala *et al.* studied the nonlinear optical properties of **G-QDs** and found that zigzag edges **QDs** show interesting optical properties.[32] The tunability of the emission of **QDs** has been recently analysed considering the effect of different functional groups.[18]

Herein, we evaluate the effect of the OH functionalisation on the ionisation potentials, absorption and emission properties of **GO-QDs** zigzag edge models. Our results show a clear strategy to tune the properties of **GO-QDs** based on size and distribution of OH functional groups. These results contribute to a better understanding of their properties with

[a] School of Mechanical and Aerospace Engineering, Nanyang Technological University Singapore, 50 Nanyang Avenue, Singapore-639798. E-maill: krgeetha@ntu.edu.sg
[b] School of Biological and Chemical Sciences, Materials Research Institute, Queen Mary University of London, Mile End Road, London E1 4NS, UK. E-mail: [c] r.crespo-otero@qmul.ac.uk

Electronic Supplementary Information (ESI) available:[details of any supplementary information available should be included here]. See DOI: 10.1039/x0xx00000x

implications for the design of more efficient **GO-QDs** based devices.

B. Models and Methods

We considered different functionalisation patterns and number of OH groups on small sized zigzag **GO-QDs**. The models were built by modifying the pristine **QDs**: coronene $C_{24}H_{12}$ (**G2**), ovalene, $C_{32}H_{14}$ (**G3**) and cir-coronene $C_{54}H_{18}$ (**G4**). Considering the general composition C_nH_m, we added 2, 4, m and m+2 (**G2** and **G3**) or m+4 (**G4**) OH groups. The OH groups were added forming bonds with carbon atoms from the basal plane and substituting the hydrogens of the edge planes. Symmetrical and non-symmetrical **GO-QDs** with respect to two C_2 symmetry axes were studied based on the functionalisation patterns shown in Figure 1. Yan *et al.* showed that the most stable configurations contain epoxide and hydroxyl groups in close proximity.[16] Here, we calculated models where the hydroxyl groups are relatively close, which stabilises the surface due to the formation of hydrogen bonds. All considered models are shown in the Supporting Information.

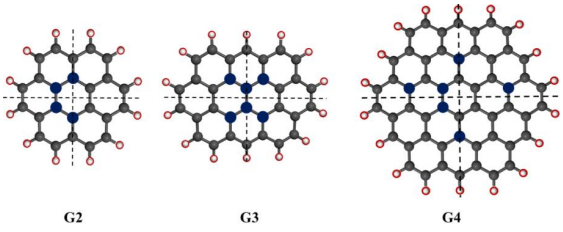

Figure 1. Pristine graphene quantum dots considered in this study. The positions considered for the axial plane substitutions are shown in red, the carbons that were functionalised with OH are shown in blue. The average radius of these **QDs** are 0.92 nm, 1.05 nm and 1.39 nm respectively.

Theoretical methods are very useful to interpret the nature of electronic excitations, but the level of theory should be carefully chosen. A proper description of charge transfer (CT) states is very important for the analysis of the mechanism of fluorescence. It has been suggested that there is an important role of the functional groups on the fluorescence mechanism of **G-QDs**.[21] To study the electronic and optical properties of the **GO-QDs**, density functional theory (DFT), linear response time-dependent functional theory (TDDFT)[33] were performed.

Two density functionals were considered, the hybrid B3LYP[34] and the long-range corrected functional ωB97X-D.[35] It is well known that typical hybrid functionals, like B3LYP, have problems to describe CT states. This problem is alleviated using long-range corrected functional like ωB97X-D,[35] which also includes dispersion correction. Time-response TDDFT calculations with ωB97X-D functional have shown a very good performance for highly delocalised molecular systems.[36,37] B3LYP is still one of most popular hybrid functional, some of the previous calculations of similar sized quantum dots have been performed with this functional. [18] Resolution of identity coupled cluster to the second order (CC2)[38] calculations were performed for the **G2** and **G2-2OH-C1** models with the def2-TZVP basis set. RI-CC2 results are in good agreement with the TDDFT calculations. A more detailed comparison of the results using different levels of theory can be found in the Supporting Information. Our discussion is based on the results obtained at TDDFT-ωB97X-D/6-311+G(d) level of theory, unless otherwise is specified.

The vertical excitations of lowest 20 excited states were calculated using TDDFT. To be able to describe diffuse excited states, we consider a triplet zeta basis set including polarisation and diffuse functions, 6-311+G(d).[39] The ground state geometries of the functionalized **GO-QDs** were optimised at B3LYP/6-311+G(d) and ωB97X-D/6-311+G(d) levels of theory. The relaxation of the geometries in S_1 was done at TDDFT-B3LYP/6-311+G(d) and TDDFT-ωB97X-D/6-311+G(d) levels of theory.

The effect of vibrations on the absorption spectra broadening was considered using the nuclear ensemble approximation[40] as implemented in Newton-X program.[41] This method considers that the spectra broadening is obtained due to the contribution of an ensemble of structures generated from a Wigner distribution based on the harmonic frequencies. 20 excited states and 200 geometries were considered to perform these simulations. Further, to analyse the effect of solvent on the electronic spectrum of **G2**, PCM method[42] was used considering cyclohexane as solvent.

The optical band gaps were calculated as the difference of energy between the ground and the first excited state.[43] The ionisation potentials were calculated as the energy difference between the cation and the neutral system. The atomic charges for the ground and the first excited states were obtained using Natural Bond Orbital (NBO) method.[44] DFT and TDDFT calculations were performed with Gaussian program[45] and CC2 calculations with Turbomole.[46]

C. Results and Discussion

Ionisation potentials

Similar to organic molecules interactions with metal surfaces in the application of self-assembled-monolayer (SAM),[47,48] **GO-QDs** can be covalently functionalized showing interesting behaviour on gold surfaces.[49] The design of efficient devices based on **GO-QDs** requires the understanding of the position of energy levels and their alignments with respect to the energy levels of molecules and metal contacts.[50] To provide an absolute reference for the electronic states of the considered **GO-QDs** models with respect to vacuum, the ionisation potentials were evaluated.

Figure 2 illustrates the shift in the energy of the excited states of selected **GO-QDs**. Functionalisation with OH groups has an important effect on the first ionisation potentials (*IP*), which are smaller than the values of the corresponding pristine **G-QDs.** This effect can be understood considering the destabilisation of the occupied molecular levels because of the incorporation of atomic orbitals from electronegative atoms, which also have an effect on the optical band gaps that are smaller than in the corresponding pristine **QDs**.

In the series **G2**, **G3**, **G4**, with the addition of aromatic rings the ionisation potentials decrease. In the case of **G2**, the

calculated ionisation potential is 7.34 eV, in very good agreement with the experimental value of 7.29 eV.[51] The calculated *IP* for **G3** is 6.65 eV, which is also in good agreement with the experimental value of 6.71 eV.[51] The calculated ionisation potential for **G4** is 6.50 eV, only slightly shifted with respect to the value for **G3**.

These calculations show a strong effect of the position of the OH groups on the electronic properties and the optical gaps (Figure 2). For **G2-2OH-C1,** the calculated *IP* is 6.34 eV, which is about 1 eV smaller than in **G2**. In the case of **G2-12OH** with edge functionalisation, and a larger number of hydroxyl groups, the *IP* is reduced to 6.52 eV. For the **G3** and **G4** based **GO-QDs**, similar effects are observed. The *IPs* for **G3-4OH-C2** and **G3-12OH** are 5.84 and 5.96 eV respectively. In the case of **G4-18OH**, the ionisation potential shifted to 6.00 eV, while the value for **G4-4OH** is 5.55 eV. In general, all examined electronic properties are more affected by functionalisation on the basal plane than edge position substitutions. We analyse the reason for this behaviour in the next sections.

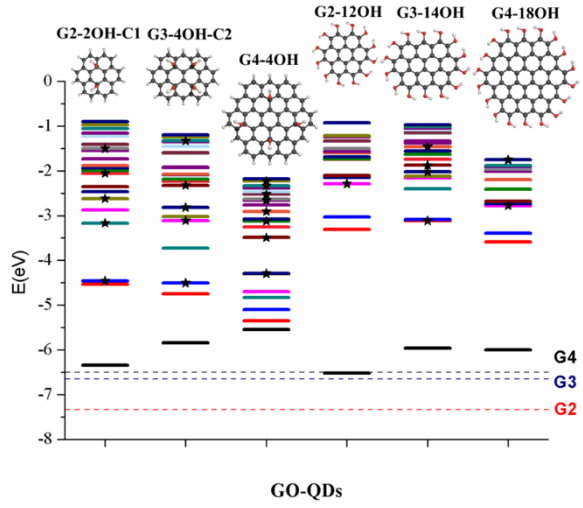

Figure 2. 20 lowest excited states for selected **GO-QDs** (TDDFT- ωB97X-D/6-311+G(d)). The electronic states were aligned with respect to vacuum, using the ionisation potentials calculated as the energy difference between the cation and the neutral **GO-QDs**. The energies of S_0 for the **GO-QDs** were shifted to the *-IP* value. The discontinuous lines show the *–IP* reference for the pristine **QDs** (**G2:** red, **G3**: blue, **G4**: black). The excited states with oscillator strengths larger than 0.1 are highlighted with stars.

Tuning of optical gaps and fluorescence

Regardless the position of the substituents, functionalisation with hydroxyl groups reduces the optical gap with respect to the values of the corresponding pristine **QDs**. Figure 3 shows the effect the optical gaps and emission energy for all considered **G2** based **QDs**. The optical gap for coronene (**G2**) with TDDFT-ωB97X-D/6-311+G(d) level of theory is 3.57 eV in very good agreement with the experimental value reported in cyclohexane which is 3.54 eV.[52] Our calculations using cyclohexane showed that the solvent does affect the first absorption band (3.57 eV).

The **GO-QDs** model with the smallest variation of optical gap values with respect to the pristine **G2** is **G2-12OH**, where all hydrogens were substituted by OH groups. The largest effect on the gaps is obtained when the **G2** is functionalised on the basal plane (**G2-2OH-C1**, **G2-2OH-C2**, **G2-4OH-C1**, **G2-4OH-C2** and **G2-12OH**).

The relaxation of the geometry on the first excited state has a very small effect on the gap because the S_1 minima are only slightly distorted with respect the Franck-Condon geometries. Emission energies show similar tendencies that the optical band gaps (Figure 3). The larger Stokes shift (0.8 eV) is obtained for **G2-2OH-C2** and it is associated with a reorientation of the hydroxyl groups.

HOMO, HOMO-1, LUMO and LUMO+1 frontier orbitals have the most important contributions to S_1. The features of these orbitals do not change significantly because of functionalisation (Supporting Information). The orbitals from the hydroxyl groups have a relatively small contribution to the frontier orbitals as it can be seen in the case of **G2-2OH-C1** and **G2-12OH**. For **G2**, the main electronic transitions involved in S_1 are HOMO→LUMO+1 (39.8%), HOMO-1→LUMO (39.8%), HOMO→LUMO (8.2%) and HOMO-1→LUMO+1 (8.2%). Functionalisation tunes the contributions of these transitions.

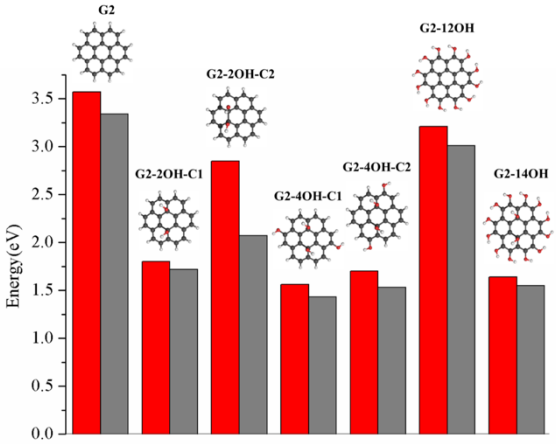

Figure 3. S_1-S_0 optical gaps (in eV) calculated at the TDDFT- ωB97X-D/6-311+G(d) level of theory for the OH **f**unctionalised quantum dots based on pristine **G2**. Red bars correspond to the vertical excitation and grey bars to the fluorescence energy

For **G2-2OH-C1,** the most important transitions are HOMO-1→LUMO (78.1%) and HOMO→LUMO+1 (9.6%). In the case of **G2-12OH,** the main electron transitions are HOMO→LUMO (34.1 %), HOMO-1→LUMO+1 (34.1%), HOMO→LUMO+1 (13.6 %) and HOMO-1→LUMO (13.6%). The first excited states show important contribution of at least two electronic transitions, consequently, the HOMO-LUMO analysis cannot provide a complete picture of these states. A detailed analysis of electron S_1-S_0 densities is discussed below in connection with the fluorescence mechanism.

Our calculations show the tuning of the optical gaps induced by basal plane functionalisation correlates with the geometry distortion. This effect can be illustrated substituting the OH groups by hydrogens in the **G2-2OH-C1** model. The obtained optical gap is 1.96 eV (1.94 eV without geometry relaxation). Considering that the optical gap for **G2-2OH-C1** is 1.80 eV, the most important effect of the basal plane functionalisation can be associated with the geometry deformation. The effect of the

functional group is minor. The distortion from the planar geometry has an important effect on the localisation of the electron densities. Calculations of charge transfer are in line with this interpretation and will be further analysed.

The effect of increasing the number of OH groups on the optical gaps also correlates with the variation of the geometries. For example, in **G2-2OH-C2**, which has the number of OH similar to **G2-2OH-C1**, but a smaller deformation of the geometry, the reduction of the optical band gap (2.82 eV) with respect to **G2** is less significant.

The effect of geometry distortion induced by edge functionalisation in elongated armchair graphene nanoflakes was examined by Cocchi *et al.* with important effects on the absorption properties.[56] Our edge functionalised **GO-QDs** do not show geometry distortion because of the small size of the OH groups, that do not induce an important steric hindrance. But some stabilisation in the system is detected due to the formation of hydrogen bonds.

Substituting the edge hydrogens in **G2-4OH-C1** and **G2-4OH-C2** has a small effect on the gaps, the values decrease to 1.56 eV and 1.70 eV, respectively. The calculated optical band gap for **G2-14OH** is 1.64 eV. This model combines the functionalisation of **G2-2OH-C1** (optical gap: 1.80 eV) and the substitutions of **G2-12OH** (optical gap: 3.21 eV), which confirms that the most important effect on the optical band gap is the distortion of the geometry induced by the hydroxyl groups.

The effect of functionalisation on larger **QDs** is illustrated for G**3** and **G4**. While increasing the size of the aromatic system reduces the optical gaps, a similar effect of functionalisation is observed. The optical gaps are shifted to the red, with a larger effect of the basal plane functionalisation. The experimental absorption spectrum for **G3** in dichloromethane (dielectric constant=8.93), shows the first band at 2.8 eV associated with the S_0-S_1 transition. The optical gap for **G3** is 3.15 eV (Figure 4), which is about 0.4 eV smaller than in **G2**. Fluorescence excitation spectrum of **G3** in a supersonic beam showed the S_1-S_0 emission band (0-0 transition) at 2.66 eV,[53] which is in very good agreement with our calculated value of 2.79 eV. This transition showed a small red solvent shift (about 0.01 eV) in 1-methylnaphthalene solvent (dielectric constant=2.7).[53]

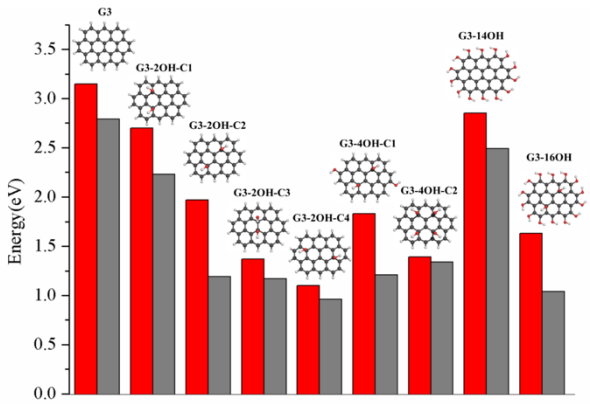

Figure 4. S_1-S_0 optical gaps (in eV) calculated at the TDDFT- ωB97X-D/6-311+G(d) level of theory for the OH functionalised quantum dots based on pristine **G3**. Red bars correspond to the vertical excitation and red bars to the fluorescence energy.

The largest deviation from **G3** gap is obtained for **G3-2OH-C4**, with an optical gap of 1.10 eV, which shows a more significant geometry distortion. Further functionalisation of **G3-2OH-C2** can control the optical gap depending on the position and the number of additional hydroxyl groups. For example, the substitution of two hydrogens from the edges with hydroxyl groups from **G3-2OH-C2** to **G3-4OH-C1** has a minor effect on the optical gap (1.97 eV to 1.83 eV). This effect is more important in **G3-14OH**, where all hydrogens are substituted, but the main changes with respect to **G3** are due to the functionalisation of the basal plane positions similar to **G2-14OH**.

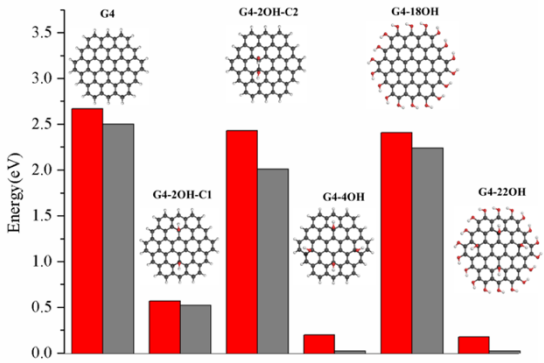

Figure 5. S_1-S_0 optical gaps (in eV) calculated at the TDDFT- ωB97X-D/6-311+G(d) level of theory for the OH **f**unctionalised quantum dots based on pristine **G4**. Blue bars correspond to the vertical excitation and red bars to the fluorescence energy.

The effect of selective functionalisation of **G4** on the optical gaps is illustrated in Figure 5. The optical gap for **G4** obtained is 2.68 eV. Symmetrical substitutions (like in **G4-2OH-C1**) imply a larger distortion in the geometry with a significant effect on the gap. The largest effect on the gaps is obtained for **G4-22OH** with similar functionalisation that in **G4-18OH** and **G4-4OH**.

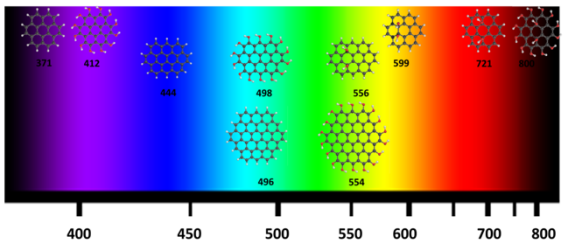

Figure 6. Calculated **G-QDs** with fluorescence in the visible (nm) (TDDFT- ωB97X-D/6-311+G(d)).

Controlling the fluorescence wavelength is very important for a wide range of applications. Small changes of the geometries in S_1 with respect to the Franck-Condon geometry were found. Consequently, the optical gaps and fluorescence energies are correlated (Figures 3-5). All considered **GO-QDs** have their fluorescence wavelength shifted to the red with respect to the corresponding pristine **G-QDs.** The substitution

of all the Franck Condon geometry edge hydrogens shifted the fluorescence about 0.3 eV with respect to the pristine **G-QDs**.

Figure 6 shows the calculated **GO-QDs** with fluorescence in the visible region. The rest of the calculated **GO-QDs** have their emission wavelength in the infrared region or lower energy regions (Supporting Information). If a significant shift is required, the basal carbons have to be functionalised. The combined effect of increasing the size of the **GO-QDs** and the selective substitution can produce crossings between S_1 and S_0. This reduction of the gap is not favourable for applications because of competition between fluorescence and non-radiative mechanisms that are more likely to happen if the gap is small. The tuning of the fluorescence and the optical gap can be explained considering the distortion of the geometry induced by the OH groups, which localises of the electron density and reduces the energy differences.

Electron-hole separation

The study of the S_1-S_0 electron density differences shows the combined effect of all involved electron transitions (Figures 7-9). This analysis also provides information about the electron-hole separation induced by the electronic excitation. It has been proposed that fluorescence of **GO-QDs** can be associated with confinement of electrons within the sp^2 electron density clusters.[18] The plots of the electron density S_1-S_0 differences show a localisation of electron density in specific regions of the **GO-QDs**. The mechanism of fluorescence of **GO-QDs**, has also been associated with the CT to and from the functional groups during the electronic transition.

Basal plane functionalisation affects the geometries of the **GO-QDs**, which are not planar due to the hybridisation of the functionalised carbons changes from sp^2 to sp^3. At the same time, the contribution of the oxygen orbitals to electronic transitions destabilises the occupied molecular orbitals. The analysis of the electronic densities of the excited state can aid in identifying which of these factors play a major role in the fluorescence mechanism. Our calculations show that the optical gap and emission is controlled by the creation of localised electron densities and that the role of CT to and from the hydroxyl groups is minor.

Functionalisation on the basal plane has an important effect on the electron-hole separation. The deformation of the geometry creates clusters with a large separation of the electro-hole. In contrast, functionalisation on the edge positions does not change significantly the distribution of the electron densities with respect to the pristine **G-QDs** (Figure 7). This explains the minor effect of functionalisation on edge positions on the optical gaps and emission energies.

For **G2** and **G2-12OH**, excitation from S_0 to S_1 transfers electron density from two-centre π(C-C) to three centres π(C-C-C), there is an important increase of electron density on the central aromatic ring (1,1).[55] That means that the electron is distributed among the central aromatic ring and the external π(C-C-C), while the hole distributed π(C-C) bonds. Only a small fraction of electron density from the hydroxyl groups is transferred to the aromatic system. To quantify the magnitude of the CT, we calculated the NBO charges in S_0 and S_1.

Our calculations show that in the case of **G2-2OH-C1**, the S_0-S_1 transition only increases the electron density of each hydroxyl oxygen about 0.013 e. For **G2-12OH**, a decrease of the electron density of about 0.004 e is found on each oxygen. In the case of **G2-14OH**, which combines edge and basal plane functionalisation, there is a small increase of the electron density on oxygen bonded to the basal C (0.011 e). The value of electron density on the hydroxyl groups depends on the position of the group. These calculations show that the CT from and to the hydroxyl groups do not play an important role in the first excited state and in the fluorescence of these **GO-QDs**.

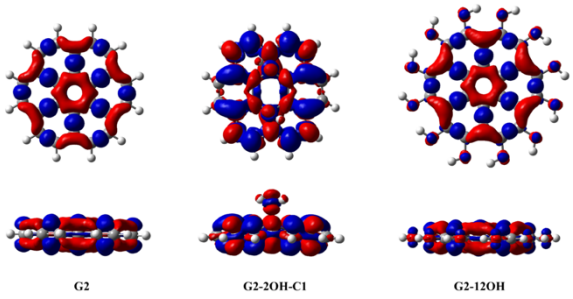

Figure 7. Difference between the S_1-S_0 electron densities (TDDFT- ωB97X-D/6-311+G(d)) for **G2**, **G2-2OH-C1** and **G2-12OH**. At the bottom, the lateral views are shown. Positive regions are in red and negative in blue. (Contours: 0.0004)

The difference of S_1-S_0 electron densities shows a different pattern in **G3** when compared to **G2**. Excitation promotes electron density from three carbon centres π(C-C-C) to π(C-C) bonds (Figure 8). In line with tuning the optical gaps, functionalisation of the edge positions (**G3-12OH**) has a small effect on the electron densities, showing a similar symmetry and patterns obtained for **G3**. Our NBO calculations also show a small electron transfer from or to the hydroxyl groups to the **GO-QDs**. In the case of **G3-2OH-C1**, the total electron transfer to the two hydroxyl groups is 0.03 e, which is larger than obtained for similar **G2** based **GO-QDs** but still very small. The transfer from OH to the aromatic system in **G3-12OH** is also small, with an electron density of only 0.05 e transfer from the **G-QD** (about 0.004 per OH group).

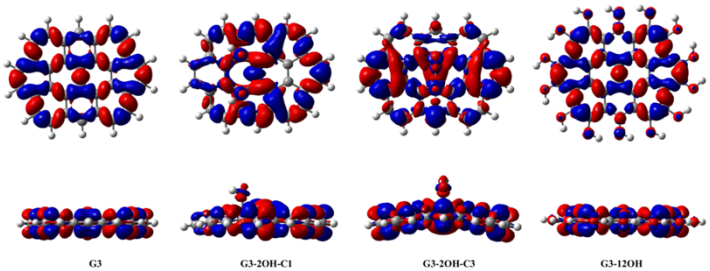

Figure 8. Difference between the S_1-S_0 electron densities (TDDFT- ωB97X-D/6-311+G(d)) for **G3**, **G3-2OH-C1**, **G3-2OH-C3** and **G3-12OH**. At the bottom, the lateral views are shown. Positive regions are in red and negative in blue. (Contours: 0.0004)

To analyse, the effect of the position of the substituent on the gaps, we consider the functionalisation with two OH groups

in the series: **G3-2OH-C1**, **G3-2OH-C2**, **G3-2OH-C3**, **G3-2OH-C4**. This series shows the important role of the position of the functionalities. Symmetrical and non-symmetrical substitutions in **G3-2OH-C1**, **G3-2OH-C3** affect the geometries and the electron densities differently (Figure 8). The analysis of the S_1-S_0 of **G3** suggests that a significant effect can be expected for **G3-2OH-C3**, where central carbons with an important electron density S_1-S_0 difference in **G3** are functionalised (Figure 8). The optical gap deviates about 2 eV from the **G3** value.

Our calculations show a small effect of the CT from or to the OH groups, with similar tendencies to the observed for **G2 GO-QDs**. In the case of functionalisation on the basal plane positions, a small electron transfer from the **GDs** can be found. For the **G3** based **G-QDs**, the maximum CT value was 0.02 e in the case of **G3-18OH**, to one of the OH bonded to a basal plane carbon. For the **G4** based **G-QDs**, the maximum CT is obtained for **G4-22OH** (0.03 e). The electron transfer from the OH on the edge positions is one order of magnitude smaller. These calculations show that the magnitude of CT from and to OH groups is very small, but there is a tendency of increasing the magnitude with the size of the **G-QDs**.

The comparison of the electron densities (S_1-S_0) differences of **G2** and **G4** shows an inverse pattern (Figure 9). The S_0-S_1 electron transition transfers electron density from the central C_6 aromatic unit (1,1) to the adjacent C-C bonds. That means that the hole has an important density on the central unit, in contrast to **G2** where the electron had a more significant density in the (1,1) central unit. Analysis of the ground state electron density using Natural Density Partitioning method shows that coronene (**G2**) has a layer of delocalised concentric pi-systems and circumcoronene (**G4**) has seven localised sextets, with only one Clar's structure.[54] This is related to the reordering of the frontier orbitals from **G2** to **G4**, where the HOMO and HOMO-1 occupied orbitals of **G2** resemble the LUMO and LUMO+1 of **G4** (Supporting Information).

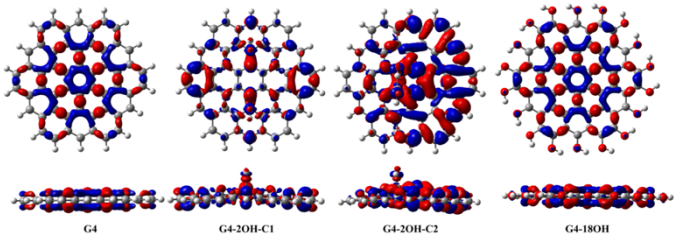

Figure 9. Difference between the S_1-S_0 electron densities (TDDFT- ωB97X-D/6-311+G(d)) for G4, G4-2OH-C1, G4-2OH-C2 and G4-18OH. At the bottom, the lateral views are shown. Positive regions are in red and negative in blue. (Contours: 0.0004)

Li *et al.* used quasiparticle calculations to analyse the effect of substitutions at one edge position of **G4** for different substituents, including OH.[26] The authors discussed the effect of orbital hybridisation and CT on the electronic structure and optical properties. Hybridisation was associated with a reduction of the gap, while CT should open the gap. In the case of OH, a significant hybridisation on the HOMO orbital was found, with a little effect on the LUMO orbital. The authors found a transfer of 0.93 e from the **QD** to the OH group with Atoms in Molecules electron partition of the electron density. To compare with their results we consider the **QD** as well (**G4-OH**) (Supporting Information).

In the ground state, we found a smaller electron transfer with NBO of about -0.2 e (-0.67 e for O and +0.47 e for H). Considering the differences in the electron densities between S_1 and S_0, only 0.002 e is transferred from the **G-QD** to the OH during the electron transition, which is in line with the small variation of the optical gap obtained for this **G-QD**. The optical band gap calculated at TDDFT-ωB97X-D/6-311+G(d) is 2.67 eV, which is only 0.01 eV shifted from the **G4-QDs**. These calculations show that the CT from and to the OH does not have an important effect on the optical gap or the fluorescence mechanism.

Higher energy excited states

Figure 2 shows that functionalisation has an important effect on the higher energy excited states. Regardless their small intensities, some intermediate states could participate in the relaxation to the ground state. For example, S_2 might be involved in the de-excitation process of all considered **GO-QDs**. Non-adiabatic dynamics simulations showed the role of the intermediate states in the relaxation of perylene esters.[57] Here, we focus on the analysis of the effect the brightest excited states, which have the most important contribution to the spectra. The effect of functionalisation on the absorption spectra is illustrated in the case of **G2-2OH-C1**.

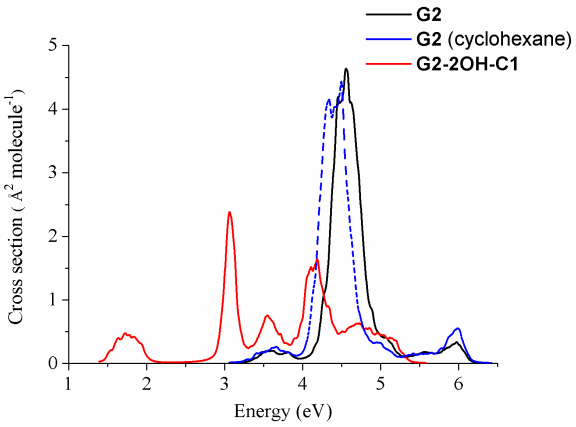

Figure 10. Spectra of **G2** and **G2-2OH-C1** quantum dots calculated at TDDFT- ωB97X-D/6-311+G(d) level of theory using the nuclear ensemble approximation.

The nuclear ensemble approximation was used to consider the effect of the vibrations on the absorption spectrum (Figure 10).[40] **G2** has only two bright states in the region between 3.5 to 6.4 eV (first 20 excited states). These states are degenerate and correspond to S_3 and S_4 (4.71 eV and oscillator strength of 1.061, symmetry D_{6h}). The predicted band associated with the first bright state transition is red-shifted about 0.2 eV (4.5 eV). While considering the solvent the band is further red-shifted about 0.1 eV (4.4 eV), which shows a much better agreement with the experimental value of 4.10 eV.[52]

The main effect of functionalisation on the spectra is the shift to the red, which is very important in the case of **G2-2OH-C1** because of the functionalisation of the basal plane carbons

(Figure 10). The first band, associated with the S_0-S_1 transition is more intense than in the pristine **G2**. The intensities of the brightest states (S_3 and S_4) are distributed among several excited states in **G2-2OH-C1** and other models. In the series: **G2**, **G2-2OH-C1**, **G2-2OH-C2**, **G2-4OH-C1**, **G2-4OH-C2**, the energies of the first bright states are 4.71 (S_3, S_4), 3.25 (S_3), 3.11 (S_3), 3.25 (S_3), 3.11 (S_3) respectively.

In general, substitutions on the basal plane positions lower the symmetry increasing the number of excited states with oscillator strengths larger than 0.1, but with smaller individual values (Supporting Information). Consequently, new features are found in the spectra (Figure 10). For **G2-12OH**, where all edge positions are functionalised with hydroxyl groups (symmetry S_6), the energies of brightest excited states are shifted to 4.23 eV (oscillator strength of 1.094) with a similar stabilisation that obtained for S_1.

In contrast to **G2** and **G4**, where S_1 has zero oscillator strength, for **G3** S_1 has an oscillator strength of 0.221 with an important contribution from the HOMO-LUMO transition (90 %). The brightest excited state is S_6 (E= 4.32 eV, oscillator strength= 1.695) followed by S_7 (E= 4.52 eV, oscillator strength= 0.429) (Supporting Information). For S_6, the main electronic transitions are HOMO→LUMO+1 (48%) HOMO-1→ LUMO (48%), while for S_7, HOMO-1→LUMO+2 transition has a contribution of 78%.

The functionalisation of the edge positions in **G3-14OH**, shifted the energies of these states to E(S_6)= 3.94 eV and E(S_7)= 4.09 eV. The energy of the brightest excited states for basal plane functionalised **GO-QDs**, are more affected. In the case **G3-16OH** which combines functionalisation on basal plane and the edge positions, the brightest excited state is S_{14} (E= 4.50 eV, oscillator strength= 0.713). There are many excited states with significant oscillator strengths, such as S_5(E= 3.34 eV, oscillator strength= 0.223), S_6(E= 3.46 eV, oscillator strength= 0.323), S_8(E=3.88 eV, oscillator strength=0.631), S_{10}(E= 4.15 eV, oscillator strength= 0.344), S_{12}(E= 4.39 eV, oscillator strength= 0.272).

For **G3** based **GO-QDs**, the energy of the brightest excited states depends significantly on the position of the functionalisation. In general, the energy of the state is shifted to the red, but some substitution patterns show a small shift or even a shift to the blue. These differences are related to the reordering of the orbitals because of functionalisation and the creation of localised electron density clusters. In the case of the **G3-2OH-C1**, **G3-2OH-C3**, **G3-2OH-C4**, the energy of the brightest excited state is shifted to the red with energies of 3.71 eV (S_6), 3.12 eV (S_4) and 3.52 eV (S_6) respectively.

In the case of **G3-2OH-C2**, where two of carbons are functionalised, the brightest states E(S_8)= 4.23 eV (oscillator strength, 0.331), E(S_9)= 4.37 eV (oscillator strength, 0.643), E(S_{13})= 4.79 eV (oscillator strength, 0.376) E(S_{15})= 4.97 eV (oscillator strength, 0.638), which are close or blue-shifted with respect to the brightest states of **G3**. If two hydroxyl groups are added to the edge positions to obtain **G3-4OH-C1**, the energy of these transitions are shifted to the red with E(S_7)= 4.05 eV (oscillator strength, 0.407), E(S_9)= 4.24 eV (oscillator strength, 0.794). Adding the hydroxyl groups symmetrically in **G3-4OH-C2** produces a pattern similar to the observed to **G3-2OH-C1**, with a further redshift, E(S_3)= 1.22 eV (oscillator strength, 1.219). These calculations show the important effect of the position of the functional groups to tune the absorption properties of these **GO-QDs**.

For the **G4**, the brightest excited states are the degenerate S_3 and S_4 with energies 3.58 eV and oscillator strengths of 1.579. For **G4-18OH**, the energies of these states are shifted to 3.22 eV (oscillator strength=1.657), which is similar to the shift for S_1. Functionalisation in the basal plane has a very strong effect on the energy levels of **G4** based **QDs**, as we already discussed in the case of S_1. For the **GO-QDs** showing the most important shifts for S_1, (**G4-2OH-C1, G4-4OH** and **G4-22OH**) the brightest states shifted to the red.

In the case of **G4-2OH-C1**, the brightest excited state is S_8 with an energy of 2.94 eV. The addition of two hydroxyl groups to obtain **G4-4OH** shifted to 2.89 eV. But several intermediate excited states showed significant intensity like S_6 (1.26 eV, oscillator strength=0.121), S_7 (2.06 eV, oscillator strength=01087), S_9 (2.43 eV, 0.1098) and S_{11} (2.64 eV, oscillator strength=0.387). The brightest excited state in **G4-22OH** is S_{13} with an energy of 2.58 eV (oscillator strength=0.559). For **G4-2OH-C2,** in the low energy region, we can find S_3, S_4 and S_5 (3.19, 3.24 and 3.60 eV) with important oscillator strengths.

Conclusions

We modelled the effect of OH-functionalisation on the electronic structure of zigzag-edge **GO-QDs**. The effects of CT and geometry distortion on the optical gaps and fluorescence mechanism were considered. Unlike previous theoretical studies on **G-QDs** that considered the features of the frontier molecular orbitals, our analysis is based on the study of electron densities of the excited states.

Our calculations clearly show that the electronic properties of **GO-QDs** can be tuned by selective functionalisation with OH groups. Functionalisation with hydroxyl groups decreases the ionisation potentials of the **GO-QDs** with respect to the associated pristine **G-QDs**. Charge transfer from and to the hydroxyl groups do not play an important role in the fluorescence mechanism. More importantly, localization of sp^2 clusters due to the distortion of the geometry controls the S_1-S_0 transitions.

We predicted that the functionalisation on the positions with larger electron-hole separation in the pristine **G-QDs** affects largely the properties. Hydroxyl groups located on the basal plane have a remarkable effect on the properties, while substitutions on the edge plane affect the properties to a minor extent. Thus our analysis offers a strategy to tune the properties of **GO-QDs** based on the distortion of the geometry and the functionalisation of positions with large electron-hole separation in the pristine **G-QDs**.

Experiments showed that reduction of oxidised **GO-QDs** blue shifted the fluorescence.[17,59] Our theoretical investigations show a similar tendency when the number of hydroxyls groups decreases from the functionalised **GO-QDs** to the corresponding pristine **G-QDs**.

Extensive functionalisation should be damaging for several applications due to the associated reduction of the optical gap and fluorescence energy, which can increase the probability of non-radiative crossings to the ground state. These results open up new opportunities for the design of OH functionalised GO-QDs for a wide range of applications.

Acknowledgements

The calculations were performed using the Queen Mary's MidPlus computational facilities, supported by QMUL Research-IT and funded by EPSRC grant EP/K000128/1 and NTU HPC clusters. RCO acknowledges the support from the School of Biological and Chemical Sciences at Queen Mary University of London.

References

1 K. P. Loh, Q. Bao, G. Eda and M. Chhowalla, *Nat. Chem.*, 2010, **2**, 1015–1024.
2 G. Eda, G. Fanchini and M. Chhowalla, *Nat. Nanotechnol.*, 2008, **3**, 270–274.
3 G. Eda and M. Chhowalla, *Adv. Mater.*, 2010, **22**, 2392–2415.
4 P. V. Kamat, *J. Phys. Chem. Lett.*, 2011, **2**, 242–251.
5 J. M. Yun, J. S. Yeo, J. Kim, H. G. Jeong, D. Y. Kim, Y. J. Noh, S. S. Kim, B. C. Ku and S. I. Na, *Adv. Mater.*, 2011, **23**, 4923–4928.
6 X. Zhu, Y. Zhu, S. Murali, M. D. Stoller and R. S. Ruoff, *ACS Nano*, 2011, 3333–3338.
7 J. William S. Hummers and R. E. Offeman, *J. Am. Chem. Soc*, 1958, **80**, 1339.
8 T. Szab, O. Berkesi, P. Forg, K. Josepovits, Y. Sanakis, D. Petridis and I. Dkny, *Chem. Mater.*, 2006, 2740–2749.
9 A. Hunt, D. A. Dikin, E. Z. Kurmaev, T. D. Boyko, P. Bazylewski, G. S. Chang and A. Moewes, *Adv. Funct. Mater.*, 2012, **22**, 3950–3957.
10 M. Z. Hossain, J. E. Johns, K. H. Bevan, H. J. Karmel, Y. T. Liang, S. Yoshimoto, K. Mukai, T. Koitaya, J. Yoshinobu, M. Kawai, A. M. Lear, L. L. Kesmodel, S. L. Tait and M. C. Hersam, *Nat. Chem.*, 2012, **4**, 305–309.
11 A. Bagri, C. Mattevi, M. Acik, Y. J. Chabal, M. Chhowalla and V. B. Shenoy, *Nat. Chem.*, 2010, **2**, 581–587.
12 C. Y. Kong, W. L. Song, M. J. Meziani, K. N. Tackett, L. Cao, A. J. Farr, A. Anderson and Y. P. Sun, *J. Supercrit. Fluids*, 2012, **61**, 206–211.
13 G. Eda, Y. Y. Lin, C. Mattevi, H. Yamaguchi, H. A. Chen, I. S. Chen, C. W. Chen and M. Chhowalla, *Adv. Mater.*, 2010, **22**, 505–509.
14 W. Gao, L. B. Alemany, L. Ci and P. M. Ajayan, *Nat. Chem.*, 2009, **1**, 403–408.
15 S. Hu, *Chem. Rec.*, 2016, **16**, 219–230.
16 J.-A. Yan, L. Xian and M. Y. Chou, *Phys. Rev. Lett.*, 2009, **103**, 086802.
17 H. Zheng, Q. Wang, Y. Long, H. Zhang, X. Huang and R. Zhu, *Chem. Commun.*, 2011, **47**, 10650.
18 M. A. Sk, A. Ananthanarayanan, L. Huang, K. H. Lim and P. Chen, *J. Mater. Chem. C*, 2014, **2**, 6954.
19 M.-H. Jang, H. D. Ha, E.-S. Lee, F. Liu, Y.-H. Kim, T. S. Seo and Y.-H. Cho, *Small*, 2015, **11**, 3773–81.
20 J. T. Robinson, S. M. Tabakman, Y. Liang, H. Wang, H. S. Casalongue, D. Vinh and H. Dai, *J. Am. Chem. Soc.*, 2011, **133**, 6825–31.
21 S. Vempati and T. Uyar, *Phys. Chem. Chem. Phys.*, 2014, **16**, 21183–203.
22 J. Peng, W. Gao, B. K. Gupta, Z. Liu, R. Romero-Aburto, L. Ge, L. Song, L. B. Alemany, X. Zhan, G. Gao, S. A. Vithayathil, B. A. Kaipparettu, A. A. Marti, T. Hayashi, J.-J. Zhu and P. M. Ajayan, *Nano Lett.*, 2012, **12**, 844–9.
23 S. S. R. K. C. Yamijala, M. Mukhopadhyay and S. K. Pati, *J. Phys. Chem. C*, 2015, **119**, 12079–12087.
24 M. Zhao, F. Yang, Y. Xue, D. Xiao and Y. Guo, *Chemphyschem*, 2014, **15**, 157–64.
25 C. Cocchi, D. Prezzi, A. Ruini, M. J. Caldas and E. Molinari, *J. Phys. Chem. C*, 2012, **116**, 17328–17335.
26 Y. Li, H. Shu, X. Niu and J. Wang, *J. Phys. Chem. C*, 2015, **119**, 24950–24957.
27 C. Cocchi, D. Prezzi, A. Ruini, M. J. Caldas and E. Molinari, *J. Phys. Chem. C*, 2012, **116**, 17328–17335.
28 M. Zhao, F. Yang, Y. Xue, D. Xiao and Y. Guo, *Chemphyschem*, 2014, **15**, 950–7.
29 I. A. Popov and A. I. Boldyrev, *European J. Org. Chem.*, 2012, **2012**, 3485–3491.
30 P. Johari and V. B. Shenoy, *ACS Nano*, 2011, **5**, 7640–7.
31 C. Cocchi, D. Prezzi, A. Ruini, M. J. Caldas and E. Molinari, *J. Phys. Chem. Lett.*, 2011, **2**, 1315–9.
32 S. S. R. K. C. Yamijala, M. Mukhopadhyay and S. K. Pati, *J. Phys. Chem. C*, 2015, **119**, 12079–12087.
33 M. E. Casida, *J. Mol. Struct. THEOCHEM*, 2009, **914**, 3–18.
34 A. D. Becke, *J. Chem. Phys.*, 1993, **98**, 5648.
35 J.-D. Chai and M. Head-Gordon, *Phys. Chem. Chem. Phys.*, 2008, **10**, 6615–20.
36 K. Sen, R. Crespo-Otero, W. Thiel and M. Barbatti, *Comput. Theor. Chem.*, 2014, **1040-1041**, 237–242.
37 K. Sen, R. Crespo-Otero, O. Weingart, W. Thiel and M. Barbatti, *J. Chem. Theory Comput.*, 2013, **9**, 533–542.
38 C. Hättig and A. Köhn, *J. Chem. Phys.*, 2002, **117**, 6939.
39 R. Krishnan, J. S. Binkley, R. Seeger and J. A. Pople, *J. Chem. Phys.*, 1980, **72**, 650.
40 R. Crespo-Otero and M. Barbatti, *Theor. Chem. Acc.*, 2012, **131**, 1237.
41 M., Barbatti, M., G. G., Ruckenbauer, F., Plasser, R., Crespo-Otero, J., Pittner, M., Persico and H. Lischka, *NEWTON-X A Packag. Newton. Dyn. close to crossing seam. Available via Internet www.newtonx.org*, 2013.
42 J. Tomasi, B. Mennucci and R. Cammi, *Chem. Rev.*, 2005, **105**, 2999–3093.
43 J.-L. Bredas, *Mater. Horiz.*, 2014, **1**, 17–19.
44 A. E. Reed, R. B. Weinstock and F. Weinhold, *J. Chem. Phys.*, 1985, **83**, 735.
45 M. J. Frisch, G. W. Trucks, H. B. Schlegel, G. E. Scuseria, M. A. Robb, J. R. Cheeseman, G. Scalmani, V. Barone, B. Mennucci, G. A. Petersson, H. Nakatsuji, M. Caricato, X. Li,

H. P. Hratchian, A. F. Izmaylov, J. Bloino, G. Zheng, J. L. Sonnenberg, M. Hada, M. Ehara, K. Toyota, R. Fukuda, J. Hasegawa, M. Ishida, T. Nakajima, Y. Honda, O. Kitao, H. Nakai, T. Vreven, J. Montgomery, J. A., J. E. Peralta, F. Ogliaro, M. Bearpark, J. J. Heyd, E. Brothers, K. N. Kudin, V. N. Staroverov, R. Kobayashi, J. Normand, K. Raghavachari, A. Rendell, J. C. Burant, S. S. Iyengar, J. Tomasi, M. Cossi, N. Rega, J. M. Millam, M. Klene, J. E. Knox, J. B. Cross, V. Bakken, C. Adamo, J. Jaramillo, R. Gomperts, R. E. Stratmann, O. Yazyev, A. J. Austin, R. Cammi, C. Pomelli, J. W. Ochterski, R. L. Martin, K. Morokuma, V. G. Zakrzewski, G. A. Voth, P. Salvador, J. J. Dannenberg, S. Dapprich, A. D. Daniels, Ö. Farkas, J. B. Foresman, J. V. Ortiz, J. Cioslowski and D. J. Fox, *Gaussian 09 C.01*.

46 R. Ahlrichs, M. Bär, M. Häser, H. Horn and C. Kölmel, *Chem. Phys. Lett.*, 1989, **162**, 165–169.

47 C. M. Crudden, J. H. Horton, I. I. Ebralidze, O. V Zenkina, A. B. McLean, B. Drevniok, Z. She, H.-B. Kraatz, N. J. Mosey, T. Seki, E. C. Keske, J. D. Leake, A. Rousina-Webb and G. Wu, *Nat. Chem.*, 2014, **6**, 409–14.

48 K. R. Geethalakshmi, X. Yang, Q. Sun, T. Y. Ng and D. Wang, *RSC Adv.*, 2015, **5**, 88625–88635.

49 A. B. Shivanandareddy, M. Kumar, V. Lakshminarayanan and S. Kumar, *RSC Adv.*, 2015, **5**, 47692–47700.

50 P. V. C. Medeiros, G. K. Gueorguiev and S. Stafström, *Phys. Rev. B*, 2012, **85**, 205423.

51 E. Clar, J. M. Robertson, R. Schloegl and W. Schmidt, *J. Am. Chem. Soc.*, 1981, **103**, 1320–1328.

52 R. Rieger, M. Kastler, V. Enkelmann and K. Müllen, *Chemistry*, 2008, **14**, 6322–5.

53 A. Amirav, *J. Chem. Phys.*, 1981, **74**, 3745.

54 I. A. Popov and A. I. Boldyrev, *European J. Org. Chem.*, 2012, **2012**, 3485–3491.

55 I. Gutman, S. J. Cyvin and V. Ivanov-Petrović, *Zeitschrift fur Naturforsch. - Sect. A J. Phys. Sci.*, 1998, **53**, 699–703.

56 C. Cocchi, D. Prezzi, A. Ruini, M. J. Caldas and E. Molinari, *J. Phys. Chem. C*, 2012, **116**, 17328–17335.

57 J. Vollbrecht, C. Wiebeler, A. Neuba, H. Bock, S. Schumacher and H. Kitzerow, *J. Phys. Chem. C*, 2016, **120**, 7839–7848.

58 R. Waris, M. A. Rembert, D. M. Sellers, W. E. Acree, K. W. Street, C. F. Poole, P. H. Shetty and J. C. Fetzer, *Appl. Spectrosc.*, 1988, **42**, 1525–1531.

59 C.-T. Chien, S.-S. Li, W.-J. Lai, Y.-C. Yeh, H.-A. Chen, I.-S. Chen, L.-C. Chen, K.-H. Chen, T. Nemoto, S. Isoda, M. Chen, T. Fujita, G. Eda, H. Yamaguchi, M. Chhowalla and C.-W. Chen, *Angew. Chemie Int. Ed.*, 2012, **51**, 6662–6666.